ACS OMEGA

http://pubs.acs.org/journal/acsodf

Article

Structural Effect of a Staggered-Blade-type Grid Spacer on the Flow and Heat Transfer Characteristics of Supercritical Water in a Triangular Core Channel

Weishu Wang,* Xiaojie Zheng, Weihui Xu, Pengfei Zhao, Ziqiang Ma, Qincheng Bi, and Xiaojing Zhu

Cite This: *ACS Omega* 2022, 7, 22714−22724

Read Online

ACCESS | Metrics & More | Article Recommendations

ABSTRACT: The flow and heat transfer characteristics of supercritical water within a triangular subchannel of a supercritical water-cooled reactor (SCWR) were numerically studied using the SSG turbulence model. The structural effect of staggered-blade-type grid spacers on the flow and heat transfer characteristics of supercritical water was analyzed. The results show that the wall temperatures calculated by the SSG model are consistent with the experimental data. The structure of the staggered-blade-type grid spacers has a significant effect on the supercritical heat transfer in the large specific heat region. The change in the inner-wall temperature and local heat transfer coefficient caused by the blocking rate at different leaf deflection angles has the same trend in the flow direction. The heat transfer coefficient peak gradually increases with an increase in deflection angle. A clear vortex is generated downstream of the grid spacer, and when the blade angle increases from 0 to 90°, the secondary flow is more obvious, and the velocity near the wall is the largest, which is about 1.99 times the center velocity. As the structure-blocking effect increases, the pressure drop in the subchannel gradually increases and the performance evaluation criteria first increase and then decrease. When using the staggered-blade-type grid spacer to improve the supercritical heat transfer effect, the spacing between adjacent grids should be ensured as far as possible, and avoid using it at the end of the channel.

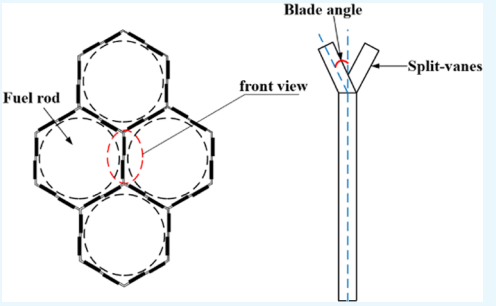

1. INTRODUCTION

Supercritical water-cooled reactor (SCWR) is a new type of safe, high-efficiency nuclear energy system based on an advanced water-cooled reactor and an innovative supercritical power generation design, which was first proposed in the 1950s. Nuclear energy system using the SCWR is efficient, simple, and safe, with zero carbon emissions. Oka[1] and Schulenberg[2] designed the concept of SCWR and analyzed its safety deeply. Scholars have conducted several research on the flow and heat transfer characteristics of supercritical water and supercritical carbon dioxide in conventional channels.[3−5] The research shows that the thermophysical properties of the supercritical working fluid change drastically in the pseudo-critical region, which determines the complexity of the heat transfer characteristics of the supercritical working fluid.[6] Shitsman[7] first discovered that the heat transfer of supercritical water deteriorated in the coal-fired tube, and Yamagata[8] investigated the enhancement of heat transfer in the pseudo-critical region. Chen[9] compared different supercritical heat transfer correlation formulas and found that these heat transfer correlation formulas were only applicable to a specific test parameter range, and the prediction error outside the experiment is relatively large. Wang[10] and Wang[11] experimentally studied the flow and heat transfer characteristics of supercritical water in internally threaded tubes, respectively. Supercritical water heat transfer is complex and influenced by multiple parameters. Near the quasi-critical region, the physical properties of supercritical water have changed dramatically. Its specific heat increases sharply, while its density, viscosity, and thermal conductivity drop sharply. Its flow and heat transfer characteristics are completely different from conventional single-phase flow and two-phase flow. In addition, most studies on the heat transfer and flow characteristics of supercritical fluids are aimed at the flow and heat transfer in round tubes, However, in the SCWR core heat exchange, the heat is generated by the fuel rods and used to heat the working fluid flowing between the rod bundles. The interpretations of the pseudo-critical region heat transfer mechanism and the correlation of supercritical heat transfer prediction are inconsistent, and thermal parameters and channel geometry have significant effects on supercritical water heat transfer.

Different from the heat transfer of supercritical water in a coal-fired boiler tube, the heat transfer law of the supercritical

Received: April 10, 2022
Accepted: June 9, 2022
Published: June 23, 2022

https://doi.org/10.1021/acsomega.2c02232
ACS Omega 2022, 7, 22714−22724

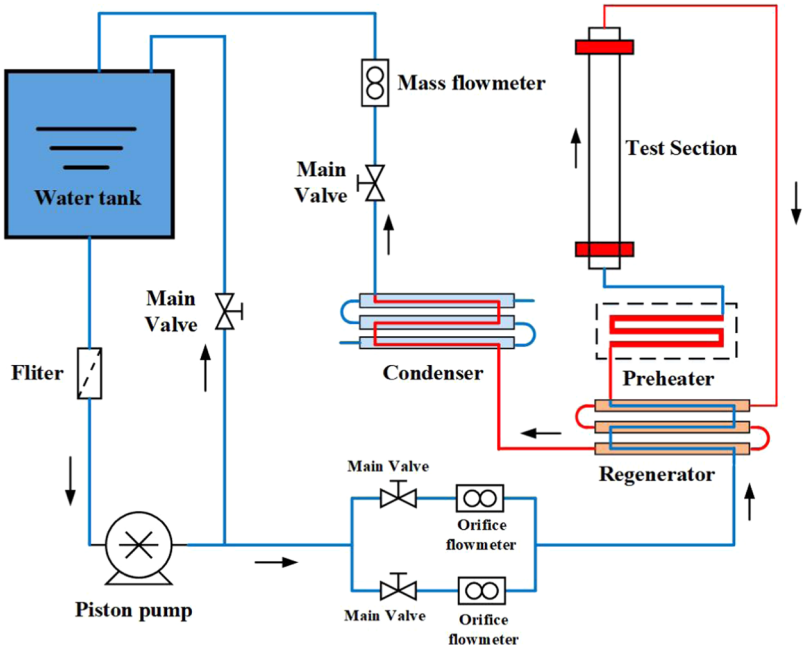

Figure 1. Schematic diagram of the supercritical pressure water loop system.

water in the coal-fired boiler tube cannot be extrapolated to predict heat transfer in the noncircular channel of the SCWR because of the uniqueness of the SCWR core channel. Many numerical and experimental studies have been conducted on the supercritical heat transfer characteristics of the SCWR. Li[12] simulated core fuel rods with electric heating rods and experimentally studied the flow heat transfer characteristics of supercritical water in a square cavity channel. Comparison of experimental data showed that the heat transfer was more enhanced at the lower supercritical pressure, but the deterioration was more likely to occur at the higher pressure. Gang[13] experimentally studied the flow and heat transfer characteristics of supercritical water in annular channel supercritical water and observed normal heat transfer and deteriorated heat transfer. Under similar flow conditions, the heat transfer coefficients for the 6 mm gap annular channel are larger than those for the 4 mm gap annular channel. Wu[14] experimentally studied the flow characteristics of supercritical water in the 2 × 2 rod bundle channel, and the results showed that the pressure drop in the pseudo-critical region and the high-enthalpy region changed significantly, and the friction factor of the 2 × 2 rod bundle was significantly larger than that of the smooth pipe. Based on a large amount of experimental data, Lv[15] proposed a heat transfer correlation formula suitable for the vertical cooling pipe of the SCWR system, and its error with experimental data is within 10%. However, experimental research is costly and time-consuming, and the influencing parameters in the experimental process are not unique. Therefore, numerical methods are widely used to study the flow and heat transfer characteristics of supercritical water with a single parameter.[16,17] Yang[18] carried out a numerical calculation on the heat transfer of supercritical water flow in a 4 m long circular tube and compared the results with the experimental results to verify the accuracy of the numerical calculation. Shang[19] used CFD software coupled with STAR-CD subroutine to conduct a numerical study on the flow and heat transfer characteristics of supercritical water in SCWR. The results show that the geometry and direction of the rod bundle have a greater impact on the wall temperature distribution and heat transfer.

The grid spacers were proposed in the concept design of the SCWR and were widely used for the precise grid of fuel components in a pressurized water reactor (PWR) and boiling water reactor (BWR), which can grid-enhance the supercritical water heat transfer and reduce the cladding temperature. Wang[20] studied the effect of spiral winding of vertically rising annular subchannels on the heat transfer of supercritical water rod bundle channels. Special attention has been focused on the effect of grid spacer on heat transfer characteristics of supercritical water. Li[21] experimentally studied the effects of grid spacer on the flow and heat transfer characteristics of supercritical water in different channels, and methods to avoid deterioration of heat transfer were proposed. Dhurandhar[22] numerically studied the heat transfer characteristics and spacer effect of R-134a under supercritical conditions in a loop tube with grid spacer. The results show that the wall temperature at the grid spacer decreases and the heat transfer coefficient increases significantly. Xiao[23] numerically studied the heat transfer characteristics of supercritical R134a in the annular channel. The study showed that the grid spacers significantly enhance the heat transfer, which can also increase the channel resistance. Different grid spacer structures affect heat transfer to different degrees and different areas.

Many studies on the flow and heat transfer characteristics of SCWR core have been carried out, and the research on the heat transfer effect of the SCWR core grid spacer has also been launched. However, there have been fewer studies on the influence of the grid spacers structure with enhanced features on the flow and heat transfer of the SCWR core. Moreover, in the application of the SCWR core grid spacer, multiple grids are generally used together, and the heat transfer effect of the multigrid core has not been studied so far. This study focuses on the flow and heat transfer rule of the geometry structure, a staggered-blade grid spacer in a triangular supercritical water subchannel, by defining the dimensionless geometry structure and longitudinal distance parameters to determine the optimal

https://doi.org/10.1021/acsomega.2c02232
ACS Omega 2022, 7, 22714−22724

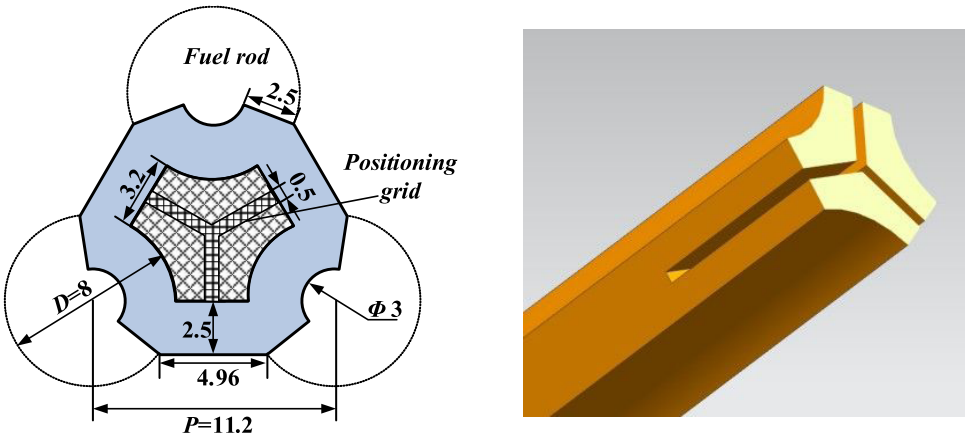

Figure 2. Schematic of test section structure. (The length of the test tube section of the triangular core channel is 1000 mm, and the structural section at the standard grid spacer is shown).

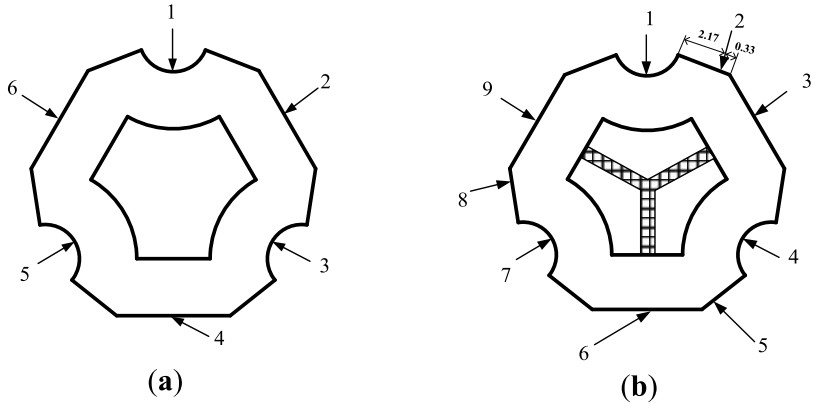

Figure 3. Arrangement of measuring points in test section: (a) arrangement of measuring points before and after grid and (b) arrangement of measuring points at grid parts. (Six measuring points were arranged in sections 1, 2, 6, and 7, as shown in (a), and the measuring points were arranged in sections 3−5, as shown in (b)).

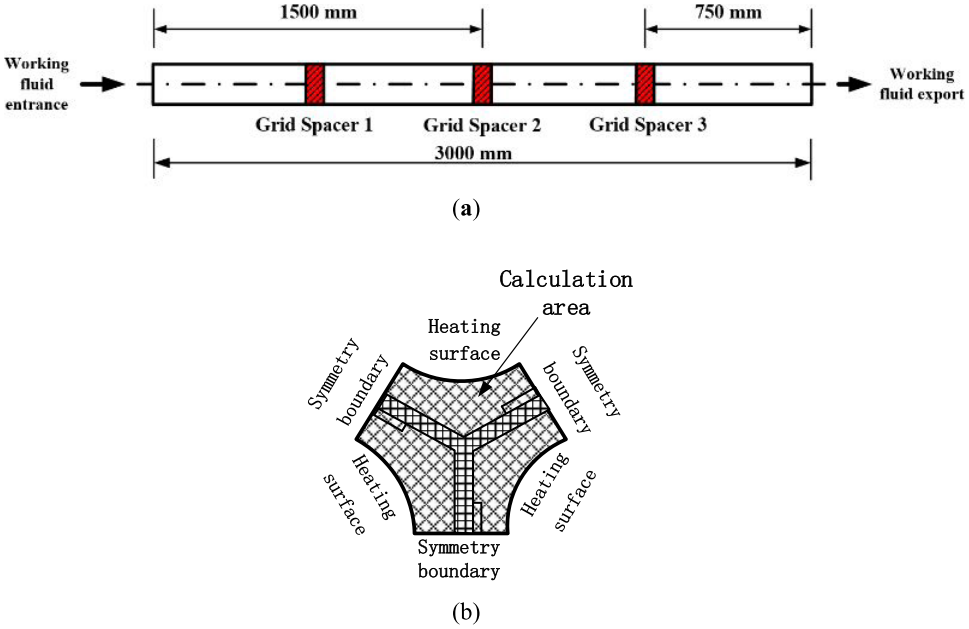

Figure 4. Schematics of core channel and calculation area: (a) grid spacer layout and (b) cross section of the calculation area. (Three grid spacers are arranged at the same interval in the core channel, as shown in (a), and the grid spacer is located in the center of the core channel, with staggered-blade strengthening features, as shown in (b)).

https://doi.org/10.1021/acsomega.2c02232
ACS Omega 2022, 7, 22714−22724

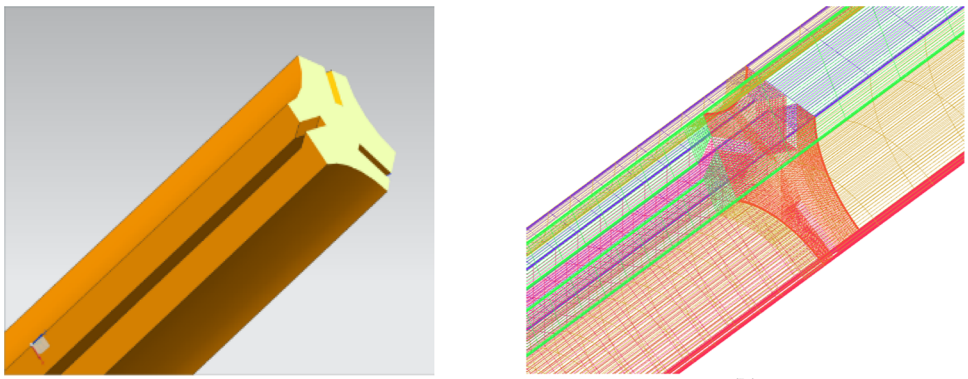

Figure 5. Physical model and meshing for numerical calculation: (a) physical model and (b) meshing. (Physical model of the staggered-blade-type grid spacer in the core channel, as shown in (a), and the grid structure of staggered-blade-type grid spacer in the core channel, as shown in (b)).

structure and layout. This research can provide a basis for the optimal design of an SCWR grid spacer. It can provide favorable theoretical support for the arrangement and structural optimization of the core grid spacer.

2. EXPERIMENTAL FACILITY AND METHODS

2.1. Experimental Loop. The experiment was completed on the high-temperature and high-pressure test stand of the State Key Laboratory of Multiphase Flow in Power Engineering at Xi'an Jiaotong University. The test system is shown in Figure 1. Deionized water was used as the test working medium, which was circulated through a plunger pump. A bypass system is provided next to the main pipeline to adjust the flow and pressure. After the deionized water passes through the filter, the pressure is boosted by the high-pressure plunger pump through the orifice flowmeter, the regenerator, and the preheater into the test section. The working fluid flows vertically upward in the test section. The test section simulates the heat release of the fuel rod by direct heating, and the test target temperature is reached by changing the heating power of the test section. The high-temperature test working fluid is condensed by the cooler and then returned to the water tank.

2.2. Test Section Geometry. The cross section of the test piece is shown in Figure 2; the grid pitch ratio P/D = 1.4, and the hydraulic diameter is 5.27 mm. The grid spacer is 50 mm long and 0.5 mm thick, and welded at the design position. The arrangement of the measuring points is shown in Figure 3.

3. NUMERICAL APPROACH

3.1. Grid Model. In the numerical calculation, the core channel of the fuel bundle length is 3000 mm and the three grid spacers are evenly arranged. The layout of the grid spacer and the calculation area are shown in Figure 4. The body length of the grid spacer is 50 mm, and the staggered blades (reinforcement feature) are located at the end of the grid spacers in the mainstream direction. The thickness of the staggered blades and the body of the grid is 0.5 mm. The triangular area between the rod bundles is the calculation area.

The Pro/E 5.0 software was used to establish a physical model of a triangular core channel with a staggered-blade grid spacer; the fluid domain was used as the calculation region. With the help of the ANSYS ICEM 14.5 software, a hexahedral meshing method was used to structure the mesh of the fluid domain. The changing boundary layer and flow field were encrypted to improve calculation accuracy. The physical model for numerical calculation and grid structure meshing division are shown in Figure 5. A schematic diagram of the bundle fuel assembly and the staggered-blade spacer grid is given in Figure 6.

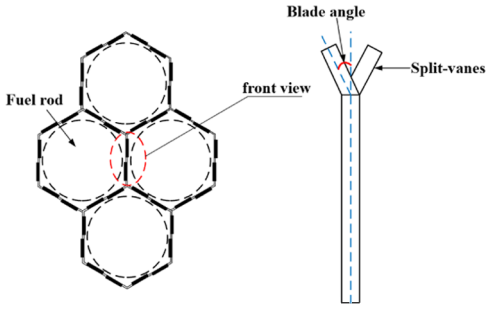

Figure 6. Sketch of structure for rod bundle with grid spacer.

3.2. Numerical Calculation Model and Boundary Conditions. In this paper, the governing N−S equation is used; the finite volume method is used to discretize the governing equation. The momentum, turbulent kinetic energy, and dissipation rate terms are discretized using the second-order upwind style. The physical properties of supercritical water are calculated by the NIST REFPROP software, which is given by the method of piecewise interpolation. The convergence criterion of the calculation variables is that the dimensionless residual is less than $1*10^{-6}$. The symmetry plane takes the symmetry boundary condition. The dimensions of the subchannel and boundary conditions are shown in Table 1.

3.3. Turbulence Model. The choice of turbulence model plays a vital role in the numerical simulation of supercritical

Table 1. Dimensions of Subchannel and Boundary Conditions

parameter/unit	value
fuel rod diameter/mm	8.0
fuel rod length/mm	3000
grid pitch ratio P/D	1.12−1.4
inlet fluid temperature/°C	250
pressure/MPa	23−28
average heat load/kW·m^{-2}	400−1000
mass flow/kg·m^{-2} s^{-1}	700−1300
blade angle/°	15, 30, 45, 60

https://doi.org/10.1021/acsomega.2c02232
ACS Omega 2022, 7, 22714−22724

fluids. Although researchers have developed more than 10 turbulence models, in view of the dramatic physical changes of supercritical water at the quasi-critical point, none is universally applicable to accurately predict heat transfer in supercritical water. Based on numerous research results of researchers, the SSG turbulence model best predicts the supercritical fluid flow heat transfer process.[17,24] The SSG Reynolds stress model is also known as the second-order pressure-strain model, and its specific expression is shown in formula 1. In addition, the SSG turbulence model considers the effects of streamline curvature, vortex, and sudden changes in the strain rate in the flow process; it is suitable for flow field simulations with a high flow anisotropy.

$$\phi_{ij} = -(C_1\rho\varepsilon + C_1^*P)b_{ij} + C_2\rho\varepsilon\left(b_{ik}b_{jk} - \frac{1}{3}b_{mn}b_{mn}\delta_{ij}\right) + (C_3 - C_3^*\sqrt{b_{ij}b_{ij}})\rho k S_{ij} + C_4\rho k\left(b_{ik}S_{jk} + b_{ik}S_{jk} - \frac{2}{3}b_{mn}S_{mn}\delta_{ij}\right) + C_5\rho k(b_{ik}\Omega_{jk} + b_{ik}\Omega_{jk}) \quad (1)$$

In formula 1, ϕ_{ij} is the pressure-strain term, b_{ij} is the Reynolds stress anisotropy tensor, defined as

$$b_{ij} = -\left(\frac{-\rho\overline{u_1u_j} + \frac{2}{3}\rho k\delta_{ij}}{2\rho k}\right) \quad (2)$$

and S_{ij} is the average strain rate, defined as

$$S_{ij} = \frac{1}{2}\left(\frac{\partial u_j}{\partial x_i} + \frac{\partial u_i}{\partial x_j}\right);\ \Omega_{ij} = \frac{1}{2}\left(\frac{\partial u_j}{\partial x_i} - \frac{\partial u_i}{\partial x_j}\right) \quad (3)$$

Constant: $C_1 = 3.4$, $C_1^* = 1.8$, $C_2 = 4.2$, $C_3 = 0.8$, $C_3^* = 1.3$, $C_4 = 1.25$, $C_4 = 0.4$.

Figure 7 shows the inner-wall temperature obtained by the SSG turbulence model at the standard grid spacer when the pressure P = 25 MPa, the heat flux density q = 400 kW/m^2, and the mass flow rate G = 1000 kg/(m^2·s). Meanwhile, the comparison of numerical simulation results and the experimental data is also shown in Figure 7. It indicates that the SSG turbulence model of supercritical water flow heat transfer considering the wall temperature of the grid spacer core channel is consistent with the experimental data. In fact, the turbulence and cross-flow of supercritical water flow in the channel caused by the staggered-blade structure locator are complex. The SSG turbulence model can predict this complex flow field, ensuring the reliability of the numerical simulation calculation results.

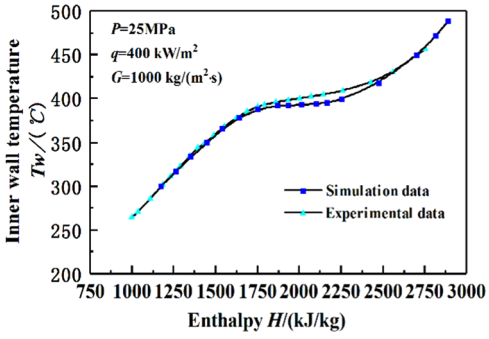

Figure 7. Comparison of numerical simulation and experimental data.

3.4. Grid Sensitivity Analysis. To ensure the reliability of numerical simulation, a high-quality mesh of a sufficient number is established by dividing the boundary layer near the solid heating surface and performing grid encryption at the grid spacer. Because the axial distance of the calculation area is considerably long, the size and number of meshes near the wall must be adjusted accordingly; that is, the number of radials and axial mesh nodes is changed. An appropriate boundary layer number and boundary division method is chosen to obtain a grid that provides high calculation accuracy. In addition, by changing the thickness of the boundary layer and comparing the y+ numbers of different near-wall grids, the heat transfer coefficient changes with the enthalpy value, and grid-independent solutions can be obtained. Table 2 shows the minimum near-wall y+ number, boundary layer number, and the total number of meshes corresponding to different meshing methods.

Table 2. Grid Independence Verification Study

scheme	minimum near-wall y+	number of boundary layers	total number of grids
1	10	5	702 500
2	5	8	760 000
3	0.1	10	947 500
4	0.04	12	1 010 000

Figure 8 shows the influence of the four meshing methods on the local heat transfer coefficient when the pressure P = 23 MPa, the heat flux density q = 1000 kW/m^2, and the mass flow rate G = 600 kg/(m^2·s). The simulations are all based on the Reynolds stress SSG $k-\omega$ turbulence model, with good applicability. Figure 8 indicates that the results corresponding to different meshing methods are not significantly different. In the mainstream enthalpy zone, there is little difference between the calculation results of schemes 3 and 4, and a further increase in the number of grids has essentially no effect on the results. Thus, the grid division method of scheme 3 is adopted to ensure the reliability and accuracy of the numerical calculation results.

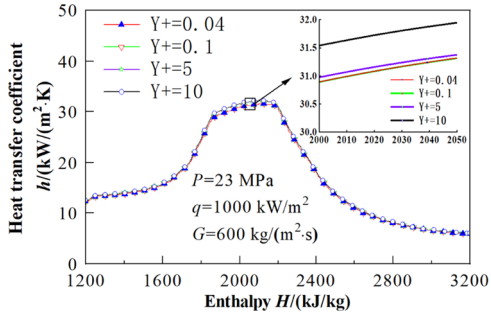

Figure 8. Comparison of heat transfer coefficient with enthalpy value at given y+.

4. RESULTS AND DISCUSSION

4.1. Geometric Structure of the Staggered-Blade. To strengthen the local heat transfer, and increase the critical heat flux (CHF) of the supercritical water core channel heat transfer, the influence of different types of grid spacer and

https://doi.org/10.1021/acsomega.2c02232
ACS Omega 2022, 7, 22714−22724

staggered-blade structure declination on the flow heat transfer characteristics of triangular core channels is studied. A dimensionless parameter, flow blocking ratio e, is proposed to evaluate the geometric structure of the grid spacer and is expressed as

$$e = A_{gp}/A_{sc} \quad (4)$$

where A_{gp} is the projection of the grid spacer along the flow direction of the core subchannel and A_{sc} is the cross section of the core subchannel. The flow blocking ratio of the standard grid spacer is e_{gs}, which is 0.1625, as yielded by the flow blocking ratio expression.

The structures of the staggered-blade locators with different blade angles and flow blocking ratios are shown in Table 3.

Table 3. Structure and Description of Different Flow Blocking Ratios

serial number	blade angle (°)	flow blocking ratio e	grid spacer geometry
1		0	no grid piece
2	15	0.2157	interleaving the flow direction of the blade angle of 15°
3	30	0.2653	interleaving the flow direction of the blade angle of 30°
4	45	0.3078	interleaving the flow direction of the blade angle of 45°
5	60	0.3405	interleaving the flow direction of the blade angle of 60°

The deviating angles of the staggered blades and the flow direction are 15, 30, 45, and 60°, respectively. The grid spacers with different blade deflection angles are shown in Figure 9.

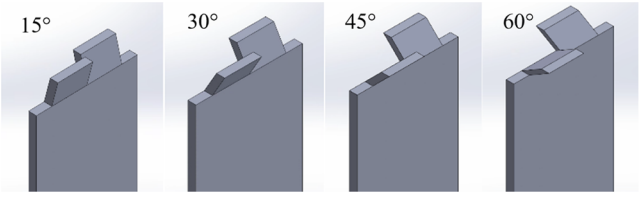

Figure 9. Shapes of the split-vanes.

4.2. Influence of Flow Blocking Ratio on Heat Transfer. Figure 10 shows the influences of the longitudinal distance of grid on heat transfer characteristics at the pressure P = 25 MPa, the mass flow rate G = 700 kg/(m^2·s), and the heat flux density q = 600 kW/m^2; including the axial distribution of the inner-wall temperature and heat transfer coefficient when the longitudinal distance of grid is 500, 600, and 750 mm.

Figure 10 demonstrates that the temperature distribution of the inner wall and the heat transfer coefficient of the channel axially fluctuates at the grid spacer, and the disturbance effect of the grid spacer on the inner-wall temperature along the direction of fluid flow gradually weakens, but the heat transfer coefficient gradually increases. When the fluid in the channel flows through the grid spacer, the cross-sectional area of the channel suddenly becomes smaller, the fluid velocity increases, the heat exchange between the fluid and the wall surface is accelerated, and the wall surface temperature decreases.

As can be seen from the figure, the lattice has little effect on the heat transfer coefficient upstream of the separator but has a significant effect on the heat transfer capacity at the downstream position of the spacer. The heat transfer coefficient of $425 \leq Z/D_h \leq 450$ is much larger than other longitudinal distances of the grid, but the heat transfer is weakened in the range of $Z/D_h \geq 450$. This phenomenon may be caused by the decrease in axial velocity in the downstream area of the grid. In the area downstream of the second grid spacer, the temperature of the inner wall decreases gradually and the temperature of the inner-wall downstream of the front and rear grid spacers increases in varying degrees. Near the second grid spacer, the working medium reaches the pseudo-critical temperature, the superheated water's specific pressure heat capacity is at a peak value much higher than the corresponding heat of the adjacent water, the density and dynamic viscosity decrease sharply, and the special physical properties that cause the fluid to absorb heat are stronger, which effectively reduces the temperature of the heating wall.

Due to the large temperature difference between the fluid and the heating wall at the inlet grid spacer, the flow velocity of the fluid downstream of the grid spacer decreases and the wall temperature increases rapidly. The fluid at the end of the grid spacer is further heated to a value above the critical temperature. Considering the influence of longitudinal distance of grid on enhanced heat transfer, the use of staggered-blade-type grid spacers in high-temperature areas should be avoided. The specific heat decreases sharply and the heat exchange

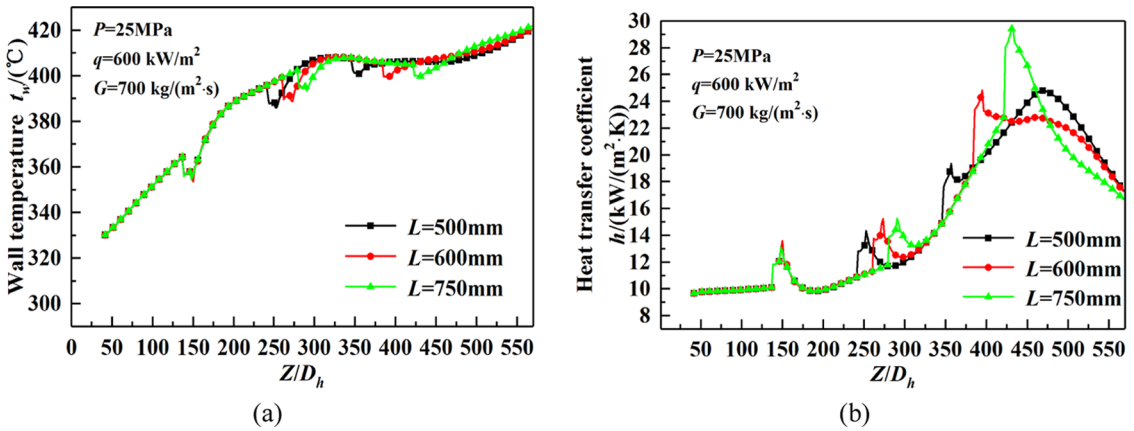

Figure 10. Effect of the longitudinal distance of grid on heat transfer characteristics. (a) Axial distribution of inner-wall temperature and (b) axial distribution of heat transfer coefficient.

https://doi.org/10.1021/acsomega.2c02232
ACS Omega 2022, 7, 22714−22724

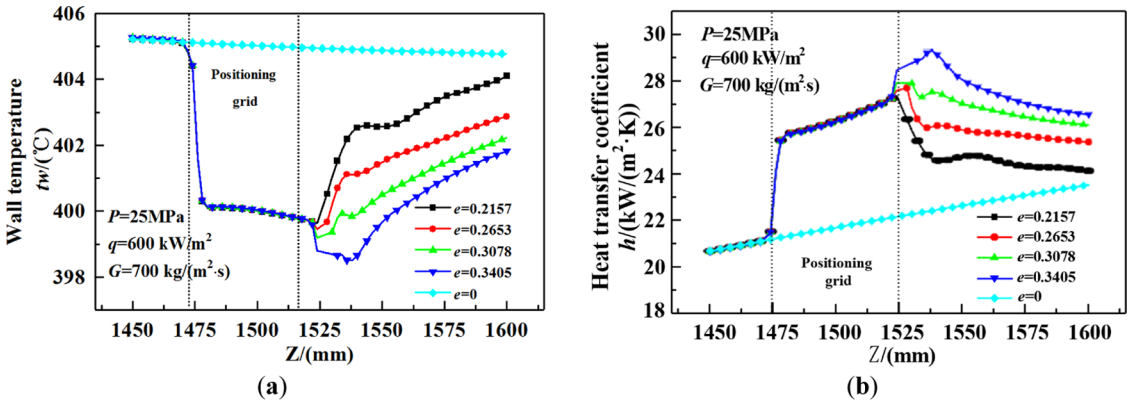

Figure 11. Effect of flow blocking ratio on local heat transfer characteristics: (a) temperature on the inner wall of the locator and (b) local heat transfer coefficient of the locator.

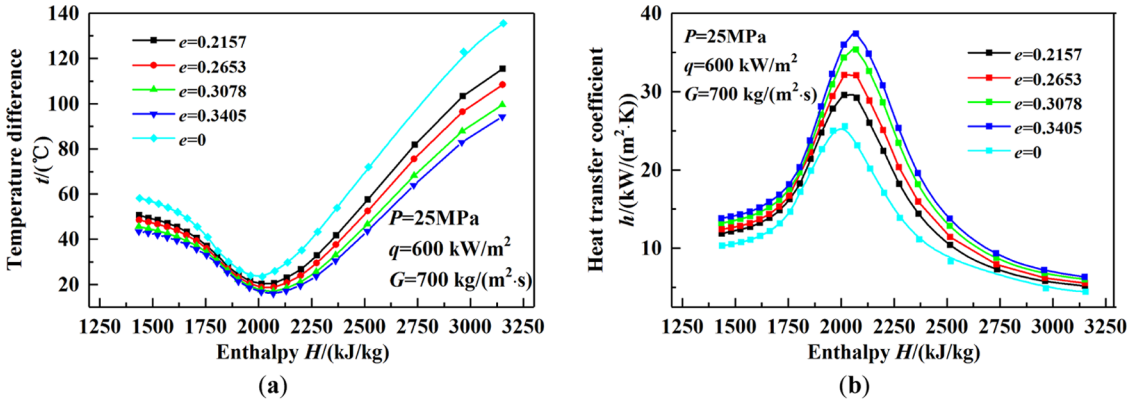

Figure 12. Effect of flow blocking ratio on transfer characteristics: (a) change in temperature according to enthalpy and (b) change in heat transfer coefficient according to enthalpy.

energy level between the fluid and the wall surface decreases, leading to an increase in the wall surface temperature. This shows that the heat exchange effect between the fluid and the wall surface is the best in the vicinity of the second grid spacer. Thus, it is the key area of the structural effect of the grid spacer.

The structural effect of the staggered-blade grid is analyzed mainly through the local enhanced heat transfer characteristics of different blade angles at the end of the grid spacer. Figure 11 shows that when the pressure P = 25 MPa, the heat flux density q = 600 kW/m^2, and the mass flow rate G = 700 kg/(m^2·s), the flow blocking ratio affects the local heat transfer downstream of the grid spacer.

Figure 11 illustrates that the local heat transfer coefficient between the fluid and the tube wall increases first and then decreases along the fluid flow direction when the working medium flows through the grid spacer. The peak appears at the end of the grid spacer and is much higher than the heat transfer coefficient in the smooth channel without a grid spacer. The changing trend of the inner-wall temperature along the flow direction is exactly opposite to the trend of the local heat transfer coefficient, indicating that the staggered-blade grid spacer has a significant effect in locally enhancing heat transfer and effectively reducing wall temperature. This is due to the influence of the angle of the blade at the end of the grid spacer. The strengthening feature at a certain blade declination greatly enhances the disturbance of the fluid flowing through it, increasing the convective heat transfer between the supercritical water and the cladding tube wall. The local heat transfer coefficient peaks at the end of the grid spacer, and the corresponding inner-wall temperature reaches a minimum. In addition, upon gradually increasing the deflection angle of the staggered blades of the grid spacer, the local heat transfer coefficient and the wall surface temperature change rule are essentially consistent. Compared with the other three grid pieces, the inner-wall temperature and local heat transfer coefficient of the grid piece with a blade angle of 45° are more continuous; a larger blade deflection angle and a greater flow blocking ratio cause the degree of turbulence at the end of the grid spacer to increase, resulting in a decrease in the axial velocity of the working fluid in the channel and reduced heat transfer.

A comparison of the flow blocking ratio is presented in Figure 12a taking into account the temperature difference between the main fluid at the grid spacer and that in the area downstream of the grid spacer. Figure 12b shows the heat transfer coefficient according to the enthalpy under the given working conditions.

In Figure 12a, the temperature difference exhibits a downward trend as the blocking rate increases in the mainstream enthalpy. In the high-enthalpy region, the temperature difference of the channel without the blocking effect increases fastest with increasing mainstream enthalpy. The temperature in the channel with the reinforced grid spacer also increases, and the corresponding wall temperature increase is larger. When the fluid flows through the grid spacer, the

https://doi.org/10.1021/acsomega.2c02232
ACS Omega 2022, 7, 22714−22724

temperature difference distribution is consistent and the value coincidence is high. With increasing mainstream enthalpy, the temperature difference decreases first and then increases, and reaches the minimum value near the quasi-critical point.

Figure 12b shows that the heat transfer coefficient reaches the maximum value near the large specific heat zone. The heat transfer coefficient of the grid spacer with strengthened features is greater than that of the smooth channel and is approximately 13.1 kW/(m^2·k). This is related to the change in the physical properties of supercritical water in regions with different enthalpy values. In the entire mainstream enthalpy area, the heat transfer coefficient has a high degree of fit with the change of enthalpy value, especially the heat transfer coefficients with blockage rates of 0.3078 and 0.3405.

The staggered-blade-type grid spacer in the subchannels of the supercritical water-cooled reactor can enhance the disturbance of the fluid downstream of the grid and enhance the heat exchange between the fluid and the heating surface. With the increase of the blade angle, the local heat transfer coefficient in the downstream of the grid increases, but the increase in the flow blocking ratio will also lead to an increase of the flow resistance in the channel. It is necessary to comprehensively consider the flow blocking ratio on the heat transfer and flow in the subchannel effect of resistance. Figure 13 indicates the variation of Nu and pressure drop at different

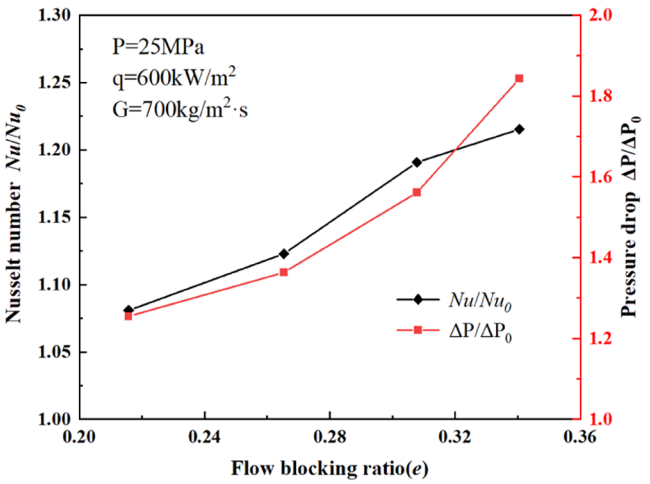

Figure 13. Effect of flow blocking ratio on Nu and pressure drop.

flow blocking ratios (subscript 0 means no spacer), and the Nusselt number is calculated by the following formula

$$Nu = hD_h/\lambda \quad (5)$$

The pressure drop and Nusselt number in the subchannel increased with the increase in the flow blocking ratio, but the rate of change was different, the flow blocking ratio increased from 0.2157 to 0.3405, the pressure drop increased from $1.25\Delta P_0$ to $1.84\Delta P_0$, the Nusselt number increased from $1.08Nu_0$ to $1.21Nu_0$. It can be seen that the increase of the flow resistance in the subchannel is greater than the increase of the heat transfer capacity.

Figure 14 shows the changes in performance evaluation criteria (PEC) under different flow blocking ratios. The definition of PEC is as follows

$$PEC = (Nu/Nu_0)/(f/f_0)^{\wedge 1/3} \quad (6)$$

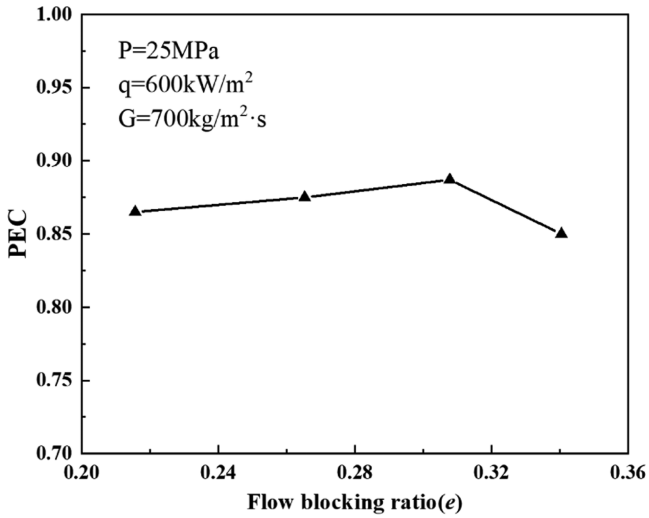

Figure 14. Effect of flow blocking ratio on PEC.

$$f = (2\Delta P D_h)/(\rho L V^2) \quad (7)$$

The change of PEC with the flow blocking ratio is that it first increases and then decreases. When the flow blocking ratio is 0.3078 (blade angle = 45°), the PEC is the highest. Although the value of PEC is less than 1, but the main function of the spacer is to provide support for the fuel rods, and the second is to improve the local heat transfer coefficient downstream of the grid and improve the safety margin of the reactor core. In the case of increasing part of the flow resistance, the heat exchange efficiency can be improved, but the extent of improvement is limited.

4.3. Structural Effects of Grid Spacer on Flow. Figure 15 shows the distribution of fluid streamlines for the four-blade deflectors in the triangular core channel.

Figure 15 indicates that the fluid velocity gradually increases along the flow direction. The velocity increase is larger after passing through the second grid spacer due to the heating of the wall, increasing of the temperature of the working fluid, and rapid decreasing of the density of the working fluid at the quasi-critical point. The streamline distribution of the fluid at the inlet is essentially the same; however, extreme turbulence occurs after it flows through the grid spacer. This is the result of the staggered blades angled at the end of the grid spacer. Disturbed by the grid spacer, the streamline bends and rotates at the end of the grid spacer. The velocity increase is larger after passing through the second grid spacer, and the radial velocity of the fluid increases. In addition, the degree of the vortex at the center of the triangular channel also gradually increases along the flow direction. Overall, the increase rate of the fluid velocity in the channels with blade angles of 45 and 60° is significantly greater than in the channels with angles of 15 and 30°. After the turbulence of the three grid spacers, the radial velocity component of the fluid continues to increase, resulting in a significant decrease in its axial velocity component. Thus, a certain length should be set aside, or a flow corrector should be used to prevent the deterioration in heat transfer at the end of the triangular channel.

Figure 16 shows the secondary flow distribution of the upstream and downstream sections and the position of the grid spacer in the triangular channel. The figure illustrates the six vortex-shaped regions with uniform symmetrical distribution formed upstream of the grid spacer at a blade angle of 15°. The

https://doi.org/10.1021/acsomega.2c02232
ACS Omega 2022, 7, 22714−22724

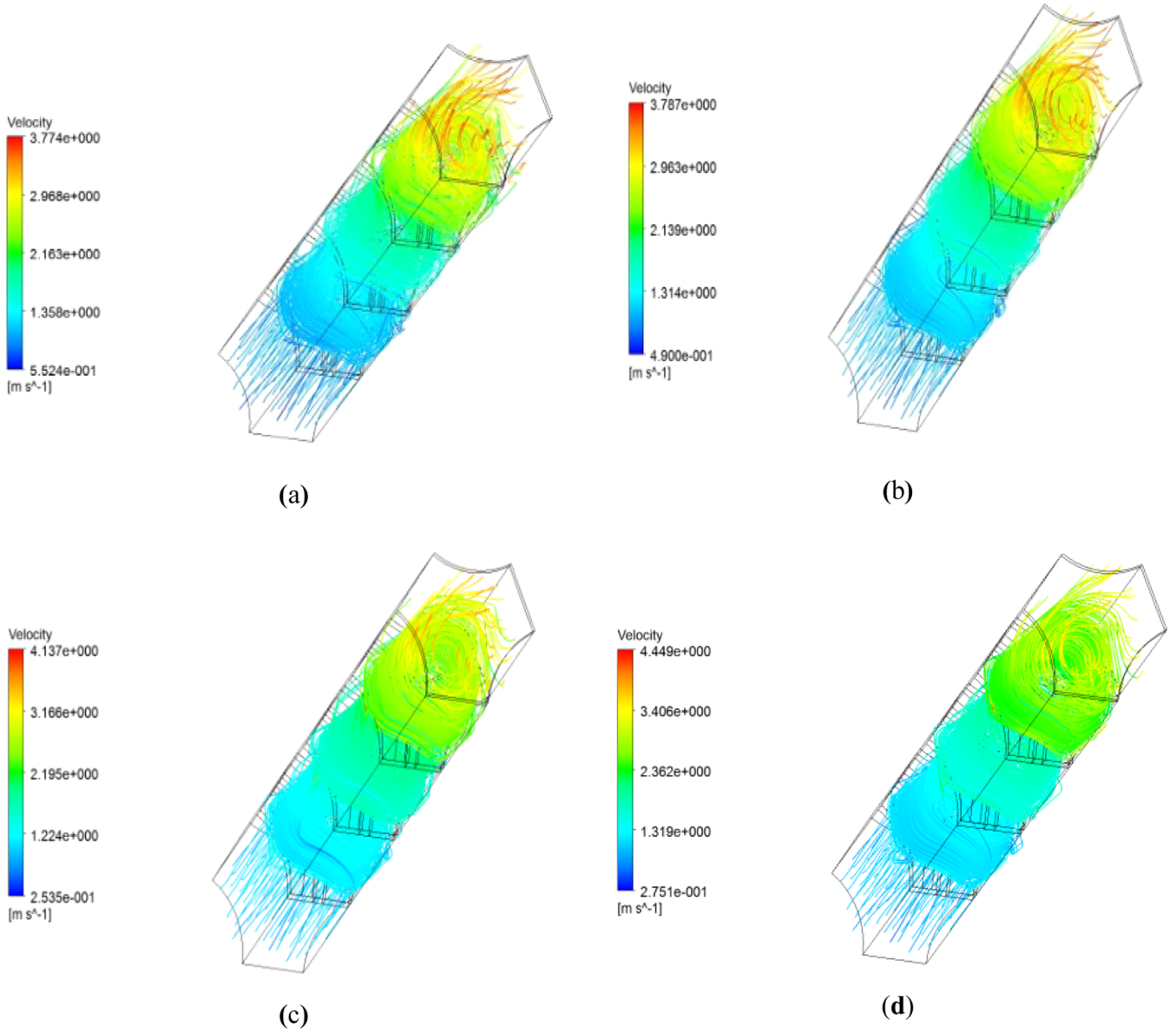

Figure 15. Streamline distribution at different leaf angles: (a) 15°; (b) 30°; (c) 45°; and (d) 60°.

vortex shapes are similar, and the vortex directions of adjacent vortices are opposite, an obvious secondary flow phenomenon. The maximum flow velocity at the cross section occurs between adjacent vortex-shaped areas, but the flow velocity in the entire cross-sectional position is not significantly different. At the cross section of the grid spacer, the cross-sectional area of the channel suddenly decreases due to the flow through the grid spacer. Thus, the fluid velocity near the grid spacer increases significantly, which promotes fluid mixing. In addition, the vortex formed upstream of the grid spacer disappears; however, the symmetry is maintained. In the area downstream of the grid spacer, a vortex flowing clockwise is formed in the center of the flow channel and the fluid velocity difference between different areas in the cross section is large. The secondary flow characteristics are more obvious. The velocity is greatest near the solid wall and is approximately 1.99 times the central velocity.

5. CONCLUSIONS

This paper presents the concepts of the blocking rate of the SCWR core grid spacer. There is an influence of dimensionless longitudinal distance and blocking ratio on the flow, and the heat transfer of supercritical water in triangular-like subchannels is studied. The primary conclusions can be summarized as follows:

(1) The staggered-blade-type grid spacer can significantly improve the supercritical heat transfer effect in the large specific heat zone. Increasing the flow blocking ratio can increase the heat transfer coefficient, which increases heat transfer but leads to an increase in fluid resistance. The heat transfer effect is the best when the flow blocking ratio is 0.3078 (blade angle = 45°).

(2) There is a vortex downstream of the grid spacer; the vortex degree becomes more obvious as it flows through the grid spacer, and the intensity of the secondary flow increases. The maximum velocity near the wall surface is approximately 1.99 times the central velocity.

https://doi.org/10.1021/acsomega.2c02232
ACS Omega 2022, 7, 22714−22724

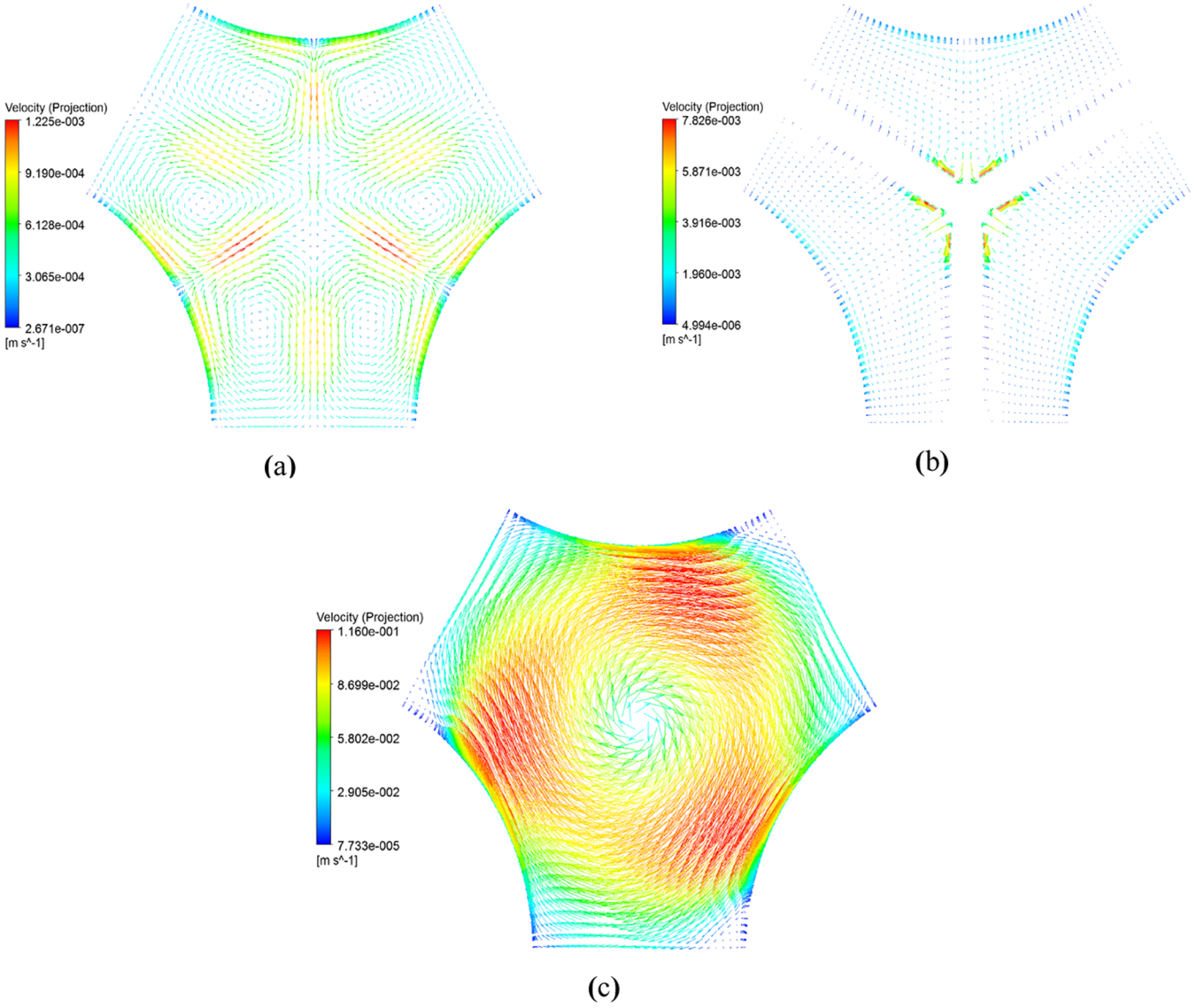

Figure 16. Distribution of secondary flow at different positions: (a) cross section of the upper part of the grid spacer; (b) cross section of the grid spacer; and (c) cross section of the lower part of the grid spacer.

(3) When arranging the core grid spacers in SCWR subchannels, the spacing should not be too small, and the use of grid spacers at the end of the channel should be avoided. Increasing the spacer spacing before the pseudo-critical temperature region is beneficial to enhance heat transfer.

AUTHOR INFORMATION

Corresponding Author

Weishu Wang − *School of Electric Power, North China University of Water Resources and Electric Power, Zhengzhou 450045, China;* orcid.org/0000-0001-7623-4047; Email: wangweishu@ncwu.edu.cn

Authors

Xiaojie Zheng − *School of Electric Power, North China University of Water Resources and Electric Power, Zhengzhou 450045, China*

Weihui Xu − *School of Electric Power, North China University of Water Resources and Electric Power, Zhengzhou 450045, China*

Pengfei Zhao − *School of Electric Power, North China University of Water Resources and Electric Power, Zhengzhou 450045, China*

Ziqiang Ma − *School of Electric Power, North China University of Water Resources and Electric Power, Zhengzhou 450045, China; State Key Laboratory of Multiphase Flow in Power Engineering, Xi'an Jiaotong University, Xi'an 710049, China*

Qincheng Bi − *State Key Laboratory of Multiphase Flow in Power Engineering, Xi'an Jiaotong University, Xi'an 710049, China*

Xiaojing Zhu − *School of Energy and Power Engineering, Dalian University of Technology, Dalian 116024, China*

Complete contact information is available at: https://pubs.acs.org/10.1021/acsomega.2c02232

Author Contributions

W.W. and W.X. contributed to conceptualization, methodology, and supervision. Formal analysis and investigation were conducted by Q.B. and X.Z. Z.M. involved in Writing—

https://doi.org/10.1021/acsomega.2c02232
ACS Omega 2022, 7, 22714−22724

original draft preparation. X.Z. and P.Z. contributed to writing—review and editing.

Funding

This project was funded by the National Natural Science Foundation of China (no. 51876024), the National Natural Science Foundation of China (no. 51976024), and the Project of Central Plains Science and Technology Innovation Leading Talents of Henan Province (no. 224200510022).

Notes

The authors declare no competing financial interest.

NOMENCLATURE

A_{sp}	projection area of grid spacer
e	flow blocking ratio
P/D	grid pitch ratio
D	rod diameter
D_h	hydraulic diameter = $4A_{sc}/P_{sc}$
G	mass flow rate
L	channel length
ρ	density
ΔP	pressure drop
PEC	performance evaluation criteria
A_{sc}	area of subchannel
e_{gs}	flow blocking ratio of standard grid spacer
p	pressure
q	heat flux density
T	temperature
Z	longitudinal distance parameter
λ	thermal conductivity
V	velocity
Nu	Nusselt number

REFERENCES

(1) Oka, Y.Review of High Temperature Water and Steam Cooled Reactor Concepts. In *Proceeding of SCR-2000* USA, 2000; pp 37−57.
(2) Schulenberg, T.; Starflinger, J. Core design concepts for high performance light water reactors. *Nucl. Eng. Technol.* **2007**, *39*, 249−256.
(3) Pioro, I. L. Current status of research on heat transfer in forced convection of fluids at supercritical pressures. *Nucl. Eng. Des.* **2019**, *354*, No. 110207.
(4) Bovard, S.; Abdi, M.; Nikou, M. R. K.; Daryasafar, A. Numerical investigation of heat transfer in supercritical CO_2 and water turbulent flow in circular tubes. *J. Supercrit. Fluids* **2017**, *119*, 88−103.
(5) Shang, Z.; Chen, S. Numerical investigation of diameter effect on heat transfer of supercritical water flows in horizontal round tubes. *Appl. Therm. Eng.* **2011**, *31*, 573−581.
(6) Zhu, B.; Xu, J.; Wu, X.; Xie, J.; Li, M. Supercritical "boiling" number, a new parameter to distinguish two regimes of carbon dioxide heat transfer in tubes. *Int. J. Therm. Sci.* **2019**, *139*, 254−266.
(7) Shitsman, M. Impairment of The Heat Transmission at Supercritical Pressures. *High Temp.* **1963**, *1*, 237−244.
(8) Yamagata, K.; Nishikawa, K.; Hasegawa, S.; Fujii, T.; Yoshida, S. Forced convection heat transfer to supercritical water flowing in tubes. *Int. J. Heat Mass Transfer* **1972**, *15*, 2575−2593.
(9) Chen, W.; Fang, X. A New Heat Transfer Correlation for Supercritical Water Flowing in Vertical Tubes. *Int. J. Heat Mass Transfer* **2014**, *78*, 156−160.
(10) Wang, W.; Bi, Q.; Gu, H.; Chen, T.; Luo, Y. An investigation on heat transfer to water flowing in vertical upward internally ribbed enhancement tube at supercritical pressure. *Adv. Sci. Lett.* **2011**, *4*, 2281−2288.
(11) Wang, J.; Li, H.; Guo, B.; Yu, S.; Zhang, Y.; Chen, T. Investigation of forced convection heat transfer of supercritical pressure water in a vertically upward internally ribbed tube. *Nucl. Eng. Des.* **2009**, *239*, 1956−1964.
(12) Li, H.; Wang, H.; Luo, Y.; Gu, H.; Shi, X.; Chen, T.; Eckart, Laurien.; Zhu, Y. Experimental investigation on heat transfer from a heated rod with a helically wrapped wire inside a square vertical channel to water at supercritical pressures. *Nucl. Eng. Des.* **2009**, *239*, 2004−2012.
(13) Gang, W.; Bi, Q.; Yang, Z.; Wang, H.; Zhu, X.; Hao, H.; Leung, K. H. Experimental investigation of heat transfer for supercritical pressure water flowing in vertical annular channels. *Nucl. Eng. Des.* **2011**, *241*, 4045−4054.
(14) Wu, G.; Wang, H.; Bi, Q. Experimental investigation of the pressure drop and friction factor of supercritical water in a 2 × 2 rod bundle. *Ann. Nucl. Energy* **2022**, *166*, No. 1087332.
(15) Lv, H.; Bi, Q.; Chen, G.; Zhang, Y.; Deng, L. Experimental study on heat transfer in vertical cooling tube cooled by downward flow in the passive heat removal system of SCWR. *Appl. Therm. Eng.* **2020**, *179*, No. 115680.
(16) Anand, S.; Sivan, S.; Santhoshkumar, D. Numerical Investigation of Supercritical Heat Transfer of Water Flowing in Vertical and Horizontal Tube with Emphasis of Gravity Effect. *J. Therm. Eng.* **2021**, *7*, 1541−1555.
(17) Qiu, Q.; Du, X.; Zhao, S.; Zhu, X.; Shen, S. Analysis of Grid Spacer Effects on the Flow and Heat Transfer of Supercritical Water Flow in an Inner Sub-channel of a SCWR Based on the Second Law of Thermodynamics. *Appl. Therm. Eng.* **2018**, *143*, 263−274.
(18) Yang, D.; Chen, J.; Feng, Y.; Chen, L. Numerical Verifications on Heat Transfer to Supercritical Water Flowing Upward in a 4 m Long Bare Vertical Tube. *Nucl. Eng. Radiat.* **2022**, *8*, 1−11.
(19) Shang, Z.; Lo, S. Numerical investigation of supercritical water-cooled nuclear reactor in horizontal rod bundles. *Nucl. Eng. Des.* **2010**, *240*, 776−782.
(20) Wang, H.; Bi, Q.; Yang, Z.; Wu, G.; Hu, R. Experimental and numerical study on the enhanced effect of spiral spacer to heat transfer of supercritical pressure water in vertical annular channels. *Appl. Therm. Eng.* **2012**, *48*, 436−445.
(21) Li, H.-b.; Zhao, M.; Hu, Z.; Zhang, Y.; Wang, F. Experimental study of supercritical water heat transfer deteriorations in different channels. *Ann. Nucl. Energy* **2018**, *119*, 240−256.
(22) Dhurandhar, S. K.; Sinha, S. L.; Verma, S. K. Spacer effects on thermal-hydraulic performance of fluid flow at supercritical pressure in annular channel-CFD methodology. *J. Mech. Eng. Sci.* **2022**, *16*, 8770−8787.
(23) Xiao, Y.; Pan, J.; Gu, H. Numerical investigation of spacer effects on heat transfer of supercritical fluid flow in an annular channel. *Int. J. Heat Mass Transfer* **2018**, *121*, 343−353.
(24) Wang, H.; Bi, Q.; L, W. Heat transfer characteristics of supercritical water in a 2 × 2 rod bundle-numerical simulation and experimental validation. *Appl. Therm. Eng.* **2016**, *100*, 730−743.

https://doi.org/10.1021/acsomega.2c02232
ACS Omega 2022, 7, 22714−22724